Ag ng 2018

PROCEEDINGS

New Engineering Concepts for Valued Agriculture

8 – 12 July 2018, Wageningen, the Netherlands

Enhanced Vineyard Descriptors combining UAV 2D and 3D Crop Models

Lorenzo Comba[b,*], Alessandro Biglia[a], Davide Ricauda Aimonino[a], Paolo Barge[a], Cristina Tortia[a], Paolo Gay[a]

[a] DiSAFA – Università degli Studi di Torino, Largo Paolo Braccini 2, 10095 Grugliasco (TO), Italy

[b] DENERG – Politecnico di Torino, Corso Duca degli Abruzzi 24, 10129 Torino, Italy

* Corresponding author. Email: lorenzo.comba@polito.it

Abstract

Precision viticulture has been assumed as an essential approach to optimise crop-managing practices and to improve the quality of food products. To deploy proper site-specific management, addressing the intrinsic variability within a vineyard or a parcel, reliable methods for features extraction and mapping of crops must be developed. The introduction in agriculture of Unmanned Aerial Vehicle (UAV), equipped with sensors able to acquire fields planar images at several wavelengths, makes available huge amount of data with high-resolution, in terms of both spatial and temporal dimension. Recently, in addition to well-known 2D mosaicked images, innovative features leaded by modern photogrammetry allowed accurate three-dimensional models of crops (ex. 3D point cloud datasets) to be generated.

The approach presented in this work is aimed at defining enhanced crop descriptors by exploiting information provided by both 2D and 3D crop models. Crucial phases of the procedure are the proper management of data provided by several sources, in order to achieve high consistency of the obtained huge dataset. In addition, the detection of vine rows, discriminating them from all the other elements of rural areas, plays a crucial role. The proposed methodology does not require the straightness of vine rows and it can be profitably applied to models of vineyards with curvilinear rows, also on steep terrains. Specific computing optimisation have been defined in order to reduce big data complexity.

A set of 24 portion of vine rows, each made by 4 plants, has been used to validate the effectiveness of the evaluated crop canopy descriptors. The 2D maps and 3D point-cloud models have been generated by using aerial images acquired during UAV flights at 35 meters high, in a study vineyard located in Serralunga d'Alba (Piedmont, Northwest of Italy). The integration of 2D-3D information allowed to obtain good performance also in the presence of dense inter-row grassing which, usually, slightly differs from vine canopies in terms of reflectance.

Keywords: crop canopy 3D models, point-cloud processing method, crop descriptors, remote sensing, precision viticulture.

1. Introduction

Precision viticulture has been assumed as an essential approach to optimise crop-managing practices and to improve the quality of food products, reducing in the meanwhile the environmental impact, such as the waste of fertilisers, pesticides, fresh water and energy (Zhang et al., 2002; Gimenez et al., 2015; Lee and Ehsani, 2015; Srbinovska et al., 2015; Reina et al., 2017).

A reliable crop monitoring procedure is the base for an effective management of precision viticulture processes. For this task, remote sensing represents a powerful technology providing huge amount of data, from which valuable information can be derived. Indeed, several interesting works discussed the evaluation of plant vigour level, radiometric indices, water stresses, grapevine size and missing plants (Meggio et al., 2010; Primicerio et al., 2015; García-Tejero et al., 2016; Tang et al., 2016; Khanal et al., 2017; Primicerio et al., 2017; Terribile et al., 2017).

A fundamental requirement for providing useful remote sensing products in agriculture is the capacity to combine high spatial resolution and quick turnaround times. In this context, an additional push in agricultural remote sensing arise from the introduction of light Unmanned Aerial Vehicle (UAV), equipped with sensors able to acquire fields planar images at several wavelengths with high and very-high resolution, in terms of both spatial and temporal dimension.

Recently, in addition to well-known 2D mosaicked images (Comba et al., 2015), innovative features leaded by modern photogrammetry allowed accurate three-dimensional models of crops (e.g. 3D point cloud datasets) to be generated. A point-cloud is a large dataset of points, referred to a geodetic reference frame, representing spots of the external surface of visible objects, where light is reflected. Data for 3D crop modelling can be directly provided by laser scanner (such as light detection and ranging systems - LiDAR) (Koening et al., 2015; Bietresato et al., 2016; Mack et al., 2017) or derived from multispectral and thermal imagery (Zarco-Tejada et al., 2014; Herrero-Huerta et al., 2015; Weiss and Baret, 2017) by photogrammetry and computer vision algorithms, such as Structure from Motion (SfM).

Several published researches proved the information potentiality of this new type of crops models for monitoring and tasks assessment in biosciences, by developing reliable algorithms to exploit 3D data in agricultural (Bendig et al., 2015; Chang et al., 2017; Malambo et al, 2018), livestock (Mortensen et al., 2016; Guo et al., 2017) and food applications (Sture et al., 2016; Su et al., 2017).

In this work, an enhanced 2D map and 3D point-cloud processing method for reliably describe the canopy status in row-layout vineyard is presented.

2. Materials and Methods

The effectiveness of the proposed approach in defining proper canopy descriptors has been evaluated on a set of 24 test areas, which are sections of vine rows made by about four plants each. The whole region where the study have been conducted covers a surface of about 1 hectares located in Diano d'Alba (Piedmont, Northwest of Italy). The region, which includes one entire vineyard parcel and part of other plots, whose latitude and longitude positions in the World Geodetic System 1984 (WGS84) range between [44.6238° 44.6242°] and [7.9988° 8.0003°] respectively (Figure 1), is characterised by a sloped land conformation, with an elevation ranging from 340 to 380 meters above sea level and a predominantly southwest orientation.

The flights paths have been planned to maintain the UAV height close to 35 meters with respect to the terrain, obtaining aerial images with a ground sample distance (GSD) of 5 cm · pixel^{-1}. The acquisition campaign has been performed close to the noon on 2017, June the 29th, using an airborne 4-bands multispectral camera (Parrot Sequoia®). In order to georeference the point-clouds in a geodetic coordinates frame, a set of 3 ground markers has been placed on selected vine trellis poles within the monitored area and their position has been accurately determined with a differential GNSS system. This methodology presented in this study uses both 2D high-resolution multispectral map and 3D point-cloud model of the crops.

2.1 Canopy descriptor from 3D point-cloud models

The vineyard 3D point-cloud model has been generated processing a set of about 400 aerial multispectral images, using Agisoft PhotoScan® software. The obtained raw 3D point-cloud model is characterised by a mean density of about 1,450 units per meter square of map surface (Figure 1).

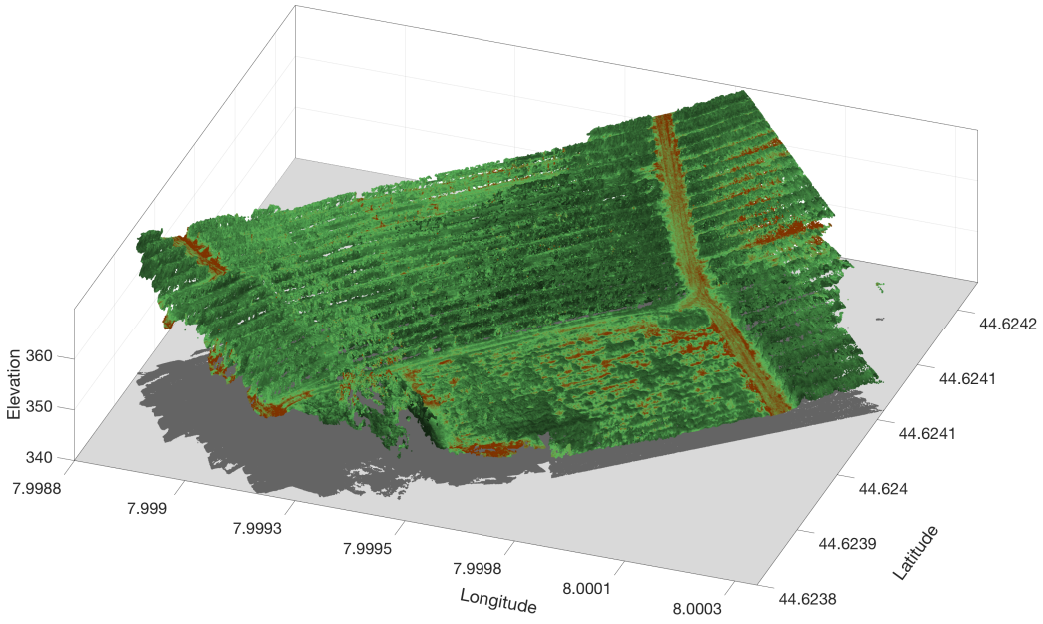

Figure 1. Point-cloud map $S^{\{WGS84\}}$ of the monitored vineyard plot (June 29th 2017).

A point-cloud map is here formally defined as a set $S^{\{WGS84\}}$ of points represented by array $p_i = \left[\varphi_i, \lambda_i, e_i\right]^T$, with $i = 1, \ldots, \mathrm{card}\left(S^{\{WGS84\}}\right)$, where φ_i, λ_i and e_i are the WGS84 latitude, longitude and elevation coordinates of point p_i respectively.

Each considered section of vine row $R_j \subset S$, with j=1,…,24, has been represented in a local Cartesian reference frame $\{\mathrm{Loc}\}_j$ in order to facilitate the subsequent processing phases, as

$$R_j^{\{\mathrm{Loc}\}_j} = \left\{ p_i = \left[x_i, \quad y_i, \quad z_i\right]^T \in \mathbb{R}^3;\ i = 1, \ldots, \mathrm{card}\left(R_j\right) \right\} \tag{1}$$

where x_i, y_i and z_i are the spatial coordinates of each point of the cloud map in meters (Figure 2a). The reference frame $\{\mathrm{Loc}\}_j$ has been defined with the x-axis aligned with the local tangent to the vine row, the z-axis with the vertical

and the y-axis accordingly to complete the frame. These local vine row information and the terrain model parameters, essential to obtain the relative height of each point of the model with respect to the local terrain surface, have been derived by the method described in Comba et. al. (2018). The origin O of $\{\mathrm{Loc}\}_j$ has been located at the soil level, aligned with a vineyard trellis close to the considered group of four vines R_j.

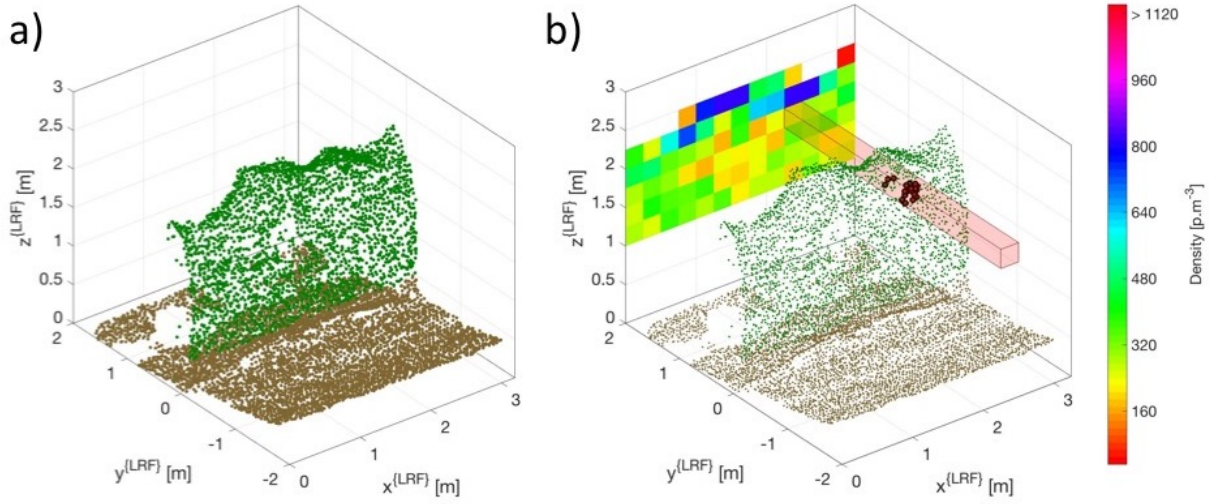

Figure 2. Portion of point-cloud $R_{13}^{\{\mathrm{Loc}\}_{13}}$ (green dots). Points belonging to subset $T_{10,4}(d)$, with $d = 0.25$ meters, are highlighted in red. Values of matrix M_{13} are graphically represented in the background (images on the x-z plane), properly aligned with x and z coordinates ranges used to compute $m_{r,s}$ values.

The 3D model of the crop canopy is here processed in order to obtain a reliable descriptor, able to represent with a single number the complex spatial distribution of the leaves along the canopy wall. Considering the point-cloud section R_j, points coordinates of which are within the ranges $0 \le x \le x_{\max}$, $0 \le y \le y_{\max}$ and $0 \le z \le z_{\max}$, an analysis of the point density variability is conducted defining a subset $T_{\mathrm{r,s}}$ of points within a parallelepiped with high and width equal to d, as

$$T_{\mathrm{r,s}}(d) = \left\{ p_i \in \mathrm{R_j} \mid (r-1)\cdot d \le x_i < r \cdot d\,,\ \ (s-1)\cdot d \le z_i < s \cdot d \right\} \tag{2}$$

with $\mathrm{r} \in \left\{1,2,\dots,\left\lceil \frac{x_{\max}}{d} \right\rceil\right\}$ and $\mathrm{s} \in \left\{1,2,\dots,\left\lceil \frac{z_{\max}}{d} \right\rceil\right\}$. In Figure 2b, a sample subset $T_{r,s}$ is highlighted in red, obtained processing section R_{22} with d equal to 0.1 meters. Indeed, considering the amount of point constituting the subset $T_{\mathrm{r,s}}(d)$, a two-dimensional map M_j can be derived as

$$M_j = \left\{ m_{r,s} = \mathrm{card}\left(T_{r,s}\right) \ \forall\, r \in \left\{1,2,\dots,\left\lceil \frac{x_{\max}}{d} \right\rceil\right\}, s \in \left\{1,2,\dots,\left\lceil \frac{z_{\max}}{d} \right\rceil\right\} \right\} \tag{3}$$

which represent the density distribution of the points of section R_j along the plane x-z. As an example, the matrix M_{13} obtained processing section R_{13} with d equal to 0.25 meters and $r \in \{1,2,\dots,13\}$ and $s \in \{1,2,\dots,6\}$ is graphically represented in Figure 2b. The obtained matrix M_j is deeply affected by the parameter d value, which is related to the specific degree of detail of the 2D canopy density distribution map. Indeed, small values of d can lead to matrix M_j better describing the canopy inhomogeneities. However, a too small value of d generates a matrix M_j with a lot of empty elements, drastically limiting the canopy wall map effectiveness. Several metrics and statistic can be defined, aimed at properly describing values of matrix M_j: in this preliminary investigation, the descriptor D_1 has been defined as the product between the average value of M_j elements and the canopy high related value $\left\lceil \frac{z_{\max}}{d} \right\rceil$, as

$$D_1(d) = \left\lceil \frac{x_{\max}}{d} \right\rceil^{-1} \cdot \sum_{r=1}^{\left\lceil \frac{x_{\max}}{d} \right\rceil} \sum_{s=1}^{\left\lceil \frac{z_{\max}}{d} \right\rceil} m_{r,s} \tag{4}$$

2.2 Canopy descriptor from 2D map and 3D model integration

In this section, the definition of a new crop descriptor derived from the fusion of 2D and 3D information of the canopy, considering both the spatial and the spectral content, is presented. The 2D multispectral map of the region has been generated with Pix4D® software, with Near Infrared, Red Edge, Red and Green spectral bands. In Figure 3a, the portion of 2D map, named I_{13}, representing the test area 13 has been plotted in the plane x-y using false colours (NIR, R, G bands), together with the section of point-clouds R_{13}. From digital number $d_{\mathrm{a,b}}$ of the test portion I_{j} of the map, with j=1,…,24, defined as $d_{\mathrm{a,b}} = [d_{NIR}\ d_{RE}\ d_R\ d_G]_{a,b}$, the well know NDVI index has been computed as $n_{\mathrm{a,b}} = \left[(d_{NIR} - d_R) \cdot (d_{NIR} + d_R)^{-1}\right]_{a,b}$. Indexes a and b point the digital number position in the image matrix, with $a \in \{1,2,\dots,A\}$, $b \in \{1,2,\dots,B\}$ and A and B that are the number of rows and columns of I_{j}. For portion I_{13}, a and b range from 1 to 80 and from 1 to 64 respectively.

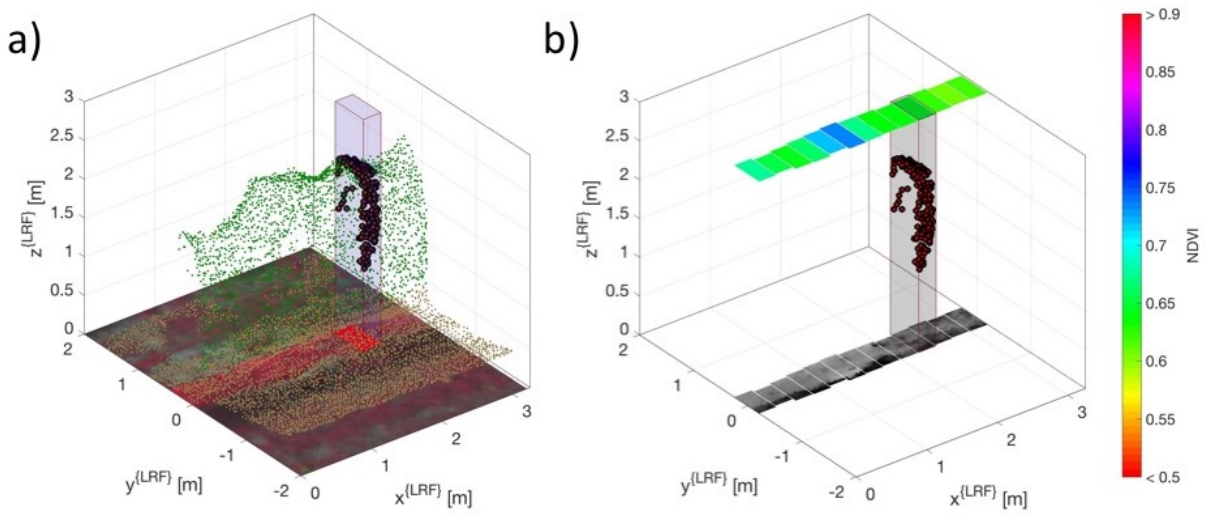

Figure 3. Portion I_{13} of the 2D multispectral map (plane x-y) of the vineyard, representing the sample area 13, with false colours (NIR, R, G bands), together with the section of point-clouds R_{13}(a). Points belonging to subset $Q_{10}(d)$, with $d = 0.25$ meters, are highlighted in red. Selected set of NDVI values H_{r} representing vines canopy, with $r \in \{1,2,\dots,13\}$, are plotted in the lower x-y plane (b), while values of array L_{13} are graphically represented in the upper the x-y plane (b).

The canopy structure and variability are evaluated selecting only pixels representing the canopy from I_{j}, by defining a subset

$$Q_{\mathrm{r}}(d) = \left\{ p_i \in \mathrm{R_j} \mid (r-1) \cdot d \le x_i < r \cdot d\,,\ 0.5 \le z_i < z_{\max} \right\} \tag{5}$$

In Figure 3a, points belonging to Q_{10}, with $d = 0.25$ meters, are highlighted in dark red, while their projection to the plane x-y are light red coloured. The region of the soil (x-y plane) occupied by the canopy is here approximated with the rectangular polygon containing the projection of all points $p_i \in Q_{\mathrm{r}}$, which is defined by $x_{\mathrm{r,min}} \le x_i < x_{\mathrm{r,max}}$ and $y_{\mathrm{r,min}} \le y_i < y_{\mathrm{r,max}}$, with $x_{\mathrm{r,min}} = \min\left(\left\{x_i : [x_{\mathrm{i}},\ y_{\mathrm{i}},\ z_{\mathrm{i}}]^{\mathrm{T}} \in Q_{\mathrm{r}}(d)\right\}\right)$, $x_{\mathrm{r,max}} = \max\left(\left\{x_i : [x_{\mathrm{i}},\ y_{\mathrm{i}},\ z_{\mathrm{i}}]^{\mathrm{T}} \in Q_{\mathrm{r}}(d)\right\}\right)$, $y_{\mathrm{r,min}} = \min\left(\left\{y_i : [x_{\mathrm{i}},\ y_{\mathrm{i}},\ z_{\mathrm{i}}]^{\mathrm{T}} \in Q_{\mathrm{r}}(d)\right\}\right)$ and $y_{\mathrm{r,max}} = \max\left(\left\{y_i : [x_{\mathrm{i}},\ y_{\mathrm{i}},\ z_{\mathrm{i}}]^{\mathrm{T}} \in Q_{\mathrm{r}}(d)\right\}\right)$. The limits of this region, in the map I_{j}, are located in pixel with indexes $a_{\mathrm{r,min}} = \left\lfloor y_{\mathrm{r,min}} \cdot w^{-1} \right\rfloor$, $a_{\mathrm{r,max}} = \left\lceil y_{\mathrm{r,max}} \cdot w^{-1} \right\rceil$,

$b_{\mathrm{r,min}} = \left\lfloor x_{\mathrm{r,min}} \cdot w^{-1} \right\rfloor$ and $b_{\mathrm{r,max}} = \left\lceil x_{\mathrm{r,max}} \cdot w^{-1} \right\rceil$, where w is the pixel spatial resolution of the 2D map. Set of pixels $n_{\mathrm{a,b}}$, defined as

$$H_{\mathrm{r}} = \left\{ n_{\mathrm{a,b}} \in I_{\mathrm{j}} \mid a \in \{ a_{\mathrm{min}},\ a_{\mathrm{min}} + 1, \dots,\ a_{\mathrm{max}} \}_{\mathrm{r}},\ \ b \in \{ b_{\mathrm{min}},\ b_{\mathrm{min}} + 1, \dots,\ b_{\mathrm{max}} \}_{\mathrm{r}} \right\} \tag{6}$$

are thus selected and the average NDVI value

$$N_{\mathrm{r}} = \left| a_{\mathrm{r,max}} - a_{\mathrm{r,min}} \right|^{-1} \cdot \left| b_{\mathrm{r,max}} - b_{\mathrm{r,min}} \right|^{-1} \cdot \sum_{a = a_{\mathrm{r,min}}}^{a_{\mathrm{r,max}}} \sum_{b = b_{\mathrm{r,min}}}^{b_{\mathrm{r,max}}} n_{\mathrm{a,b}} \tag{7}$$

computed. All values of N_{r}, with $\mathrm{r} \in \left\{ 1,2, \dots, \left\lceil \frac{x_{\mathrm{max}}}{d} \right\rceil \right\}$, for the section I_{j} are then organised in the array L_j. In Figure 3b, the selected group of pixels H_r, with $r = 1, \dots, 13$, and the graphical representation of array L_j are plotted, as an example. Several metrics and statistic can be also defined for the output of this second approach: in this preliminary investigation, the descriptor D_2 has been defined as

$$D_2(d) = \left\lceil \frac{x_{\mathrm{max}}}{d} \right\rceil^{-1} \cdot \sum_{r=1}^{\left\lceil \frac{x_{\mathrm{max}}}{d} \right\rceil} N_{\mathrm{r}} \cdot \left| y_{\mathrm{r,max}} - y_{\mathrm{r,min}} \right| \tag{8}$$

where $\left| y_{\mathrm{max}} - y_{\mathrm{min}} \right|_r$ is the local canopy width.

3. Results and Discussion

The goodness of the two vine canopy descriptors $D_1(d)$ and $D_2(d)$ from 2D aerial map and 3D point-cloud model, described in section 2, have been evaluated on 24 test areas. The set of samples have been divided in three classes on the base of the vigour and canopy density, from 'A' (lower vigour) to 'C' (higher vigour), by expert in-field visual assessment. During the manual classification, the presence of weak plants and portion of canopy wall with low leaf density and/or holes has been properly considered.

Table 1. Results of ANOVA analysis of canopy descriptor $D_1(d)$, with several values of d parameter

	Source	Sum of squares	Degrees of freedom	Mean squared error	F-statistic	*p*-value (Prob>F)
d=0.05	Groups	1022,05151	2	511,0258	11,8743	0,00035492
	Error	903,764478	21	43,0364		
	Total	1925,81598	23			
d=0.10	Groups	3634,25501	2	1817,1275	10,1404	0,00082785
	Error	3763,14287	21	179,1973		
	Total	7397,39787	23			
d=0.15	Groups	6387,88586	2	3193,9429	14,1629	0,00012765
	Error	4735,81761	21	225,5151		
	Total	11123,7035	23			
d=0.20	Groups	13119,9772	2	6559,9886	10,0490	0,00086734
	Error	13708,8268	21	652,8013		
	Total	26828,8039	23			
d=0.25	Groups	19375,3739	2	9687,6869	9,0992	0,00142558
	Error	22358,2314	21	1064,6777		
	Total	41733,6053	23			

Descriptors $D_1(d)$, with $d \in \{0.05, 0.10, 0.15, 0.20, 0.25\}$, being derived with the same approach, are not independent and their ability in describing the canopy variability has been investigated individually by ANOVA analysis. Results of the investigation are summarised in Table 1. All descriptors $D_1(d)$ prove to achieve good results, with significant differences between classes means. Descriptor $D_1(0.15)$ results to be the most performing one, obtaining the lowest *p*-value. For the sake of completeness, boxplots of the 24 samples of $D_1(0.15)$, divided in classes 'A','B' and 'C', are shown in Figure 4a.

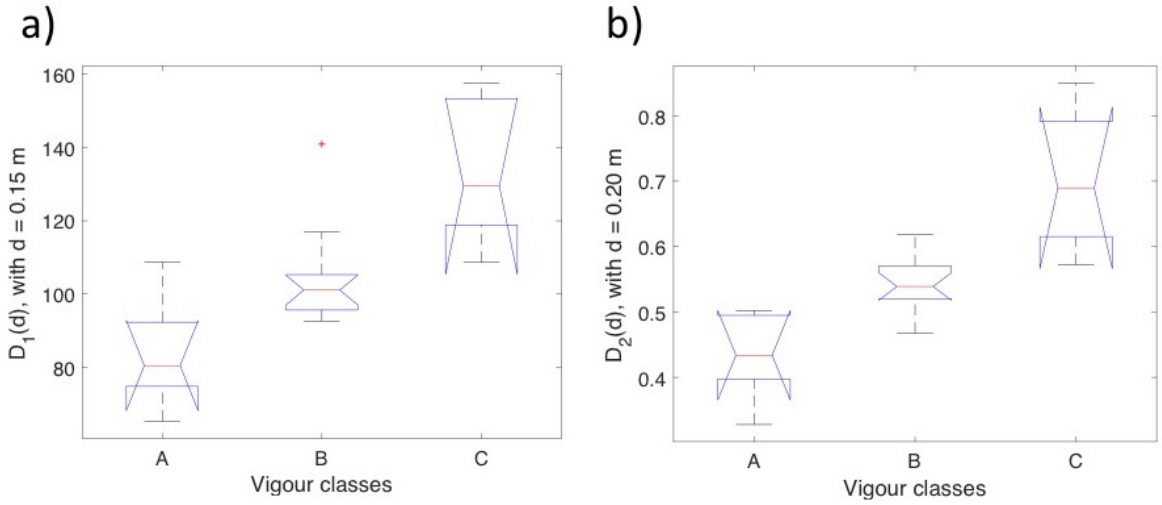

Figure 4. Boxplots of descriptor $D_1(d)$ (a), with d=0.15 meters, and of descriptor $D_2(d)$ (b), with d=0.20 meters.

The same analysis has been conducted for descriptors $D_2(d)$, with $d \in \{0.05, 0.10, 0.15, 0.20, 0.25\}$. Results of this second investigation are summarised in Table 2. All descriptors $D_2(d)$ prove to achieve good results, with significant differences between classes means. In this case, the best descriptor has been found to be $D_2(0.20)$, as shown by boxplots in Figure 4b, with the 24 samples of $D_2(0.20)$ grouped in classes 'A','B' and 'C'.

Table 2. Results of ANOVA analysis of canopy descriptor $D_2(d)$, with several values of d parameter

	Source	Sum of squares	Degrees of freedom	Mean squared error	F-statistic	p-value (Prob>F)
d=0.05	Groups	0,2052	2	0,1026	9,5531	0,0011
	Error	0,2256	21	0,0107		
	Total	0,4308	23			
d=0.10	Groups	0,1796	2	0,0898	8,2779	0,0022
	Error	0,2279	21	0,0109		
	Total	0,4075	23			
d=0.15	Groups	0,1630	2	0,0815	7,8570	0,0028
	Error	0,2179	21	0,0104		
	Total	0,3809	23			
d=0.20	Groups	0,1817	2	0,0909	20,7711	0,00001
	Error	0,0919	21	0,0044		
	Total	0,2736	23			
d=0.25	Groups	0,1557	2	0,0778	7,0401	0,0046
	Error	0,2321	21	0,0111		
	Total	0,3878	23			

A preliminary study of the combined effectiveness in using descriptors $D_1(0.15)$ and $D_2(0.20)$ to classify the canopy wall vigour has been performed implementing a binary decision tree algorithm. For this task, a cross-validation approach has been adopted, using the leave-one-out cross-validation methodology. The fraction of misclassified data resulted equal to 0.12. An improvement in classification performance can be achieved increasing the number of samples. Estimates of predictor importance have been also computed for the trained decision tree model, which confirmed the need to use both the predictor $D_1(0.15)$ and $D_2(0.20)$.

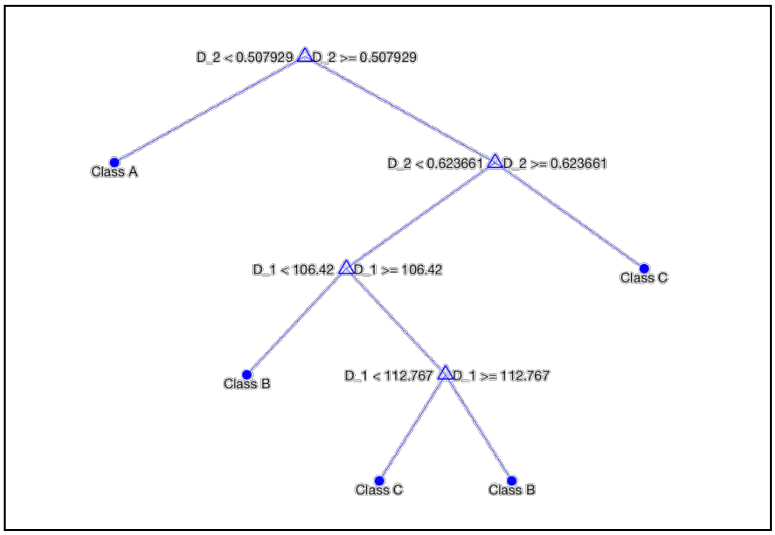

Figure 5. A decision tree diagram trained with descriptor $D_1(0.15)$ and $D_2(0.20)$.

4. Conclusions

In this work, a new methodology to process and merge data provided by vineyard 2D multispectral map and 3D point-cloud model has been presented, aimed at reliably describing the canopy status variability within row-layout vineyards. The proposed approach exploits both spatial and spectral information, with particular attention to the canopy wall analysis, in term of leaves density distribution and irregularities. Two families of crop canopy descriptor have been discussed in this study, as a function of a spatial computing parameter, in order to evaluate their effectiveness in describing vines canopy degree of growth. Analysis of variance has been used to select the more preforming ones, using a sample set made by 24 portion of vine rows. A preliminary evaluation of their classification potential has been tested training a binary decision tree model, using the leave-one-out cross-validation methodology. Obtained results are promising, although a limited number of descriptors has been still considered.

The presented data processing approach, new and with high potential, will be extended to define addition families of descriptors, evaluating the effect of several parameters. Indeed, additional crop descriptors can be used to train enhanced ensemble classifier, the effectiveness of which is strictly related to the numerosity of adopted independent variable.

Acknowledgements

This research was partially funded by project VITIFUTURE (POR FESR 2014-2020, Polo Innovazione AgriFood). The authors would like to acknowledge Germano Ettore, owner of the winery, for hosting the experimental campaign and Iway S.r.l. for supporting UAV flights.

References

Bending, J., Yu, K., Aasen, H., Bolten, A., Bennertz, S., Broscheit, J., et al., 2015. Combining UAV-based plant height from crop surface models, visible, and near infrared vegetation indices for biomass monitoring in barley. Int J Appl Earth Obs 39, 79 - 87.

Bietresato, M., Carabin, G., Vidoni, R., Gasparetto, A., Mazzetto, F., 2016. Evaluation of a LiDAR-based 3D-stereoscopic vision system for crop-monitoring applications. Comput Electron Agr 124, 1 - 13.

Chang, A., Jung, J., Maeda, M.M., Landivar, J., 2017. Crop height monitoring with digital imagery from Unmanned Aerial System (UAS). Comput Electron Agr 141, 232 - 237.

Comba, L., Gay, P., Primicerio, J., Ricauda Aimonino, D., 2015. Vineyard detection from unmanned aerial systems images. Comput Electron Agr 114, 78 - 87.

Comba, L., Biglia, A., Ricauda Aimonino, D., Gay, P., 2018. Unsupervised detection of vineyards by 3D point-cloud UAV photogrammetry for precision agriculture. Submitted to Comput Electron Agr.

García-Tejero, I.F., Costa, J.M., Egipto, R., Durán-Zuazo, V.H., Lima, R.S.N., Lopes, C.M. et al., 2016. Thermal data to monitor crop-water status in irrigated Mediterranean viticulture. Agr Water Manage 176, 80 - 90.

Gimenez, J., Herrera, D., Tosetti, S., Carelli, R., 2015. Optimization methodology to fruit grove mapping in precision agriculture. Comput Electron Agr 116, 88 - 100.

Guo, H., Ma, X., Ma, Q., Wang, K., Su, W., Zhu, D., 2017. LSSA_CAU: An interactive 3d point clouds analysis software for body measurement of livestock with similar forms of cows or pigs. Comput Electron Agr 138, 60 - 68.

Herrero-Huerta, M., González-Aguilera, D., Rodriguez-Gonzalvez, P., Hernández-López, D., 2015. Vineyard yield estimation by automatic 3D bunch modelling in field conditions. Comput Electron Agr 110, 17 - 26.

Khanal, S., Fulton, J., Shearer, S., 2017. An overview of current and potential applications of thermal remote sensing in precision agriculture. Comput Electron Agr 139, 22 - 32.

Koening, K., Höfle, B., Hämmerle, M., Jarmer, T., Siegmann, B., Lilienthal, H., 2015. Comparative classification analysis of post-harvest growth detection from terrestrial LiDAR point clouds in precision agriculture. ISPRS J Photogramm 104, 112 - 125.

Lee, W.S., Ehsani, R., 2015. Sensing systems for precision agriculture in Florida. Comput Electron Agr 112, 2 - 9.

Mack, J., Lenz, C., Teutrine, J., Steinhage, V., 2017. High-precision 3D detection and reconstruction of grapes from laser range data for efficient phenotyping based on supervised learning. Comput Electron Agr 135, 300 - 311.

Meggio, F., Zarco-Tejada, P.J., Núñez, L.C., Sepulcre-Cantó, G., González, M.R., Martín, P., 2010. Grape quality assessment in vineyards affected by iron deficiency chlorosis using narrow-band physiological remote sensing indices. Remote Sens Environ 114, 1968 - 1986.

Mortensen, A.K., Lisouski, P., Ahrendt, P., 2016. Weight prediction of broiler chickens using 3D computer vision. Comput Electron Agr 123, 319 - 326.

Primicerio, J., Caruso, G., Comba, L., Crisci, A., Gay, P., Guidoni, S., et al., 2017. Individual plant definition and missing plant characterization in vineyards from high-resolution UAV imagery. Eur J Remote Sens 50, 179 - 186.

Primicerio, J., Gay, P., Ricauda Aimonino, D., Comba, L., Matese, A., Di Gennaro, S. F., 2015. NDVI based vigour maps production using automatic detection of vine rows in ultra-high resolution aerial images. European Conference (10th) on Precision Agriculture, 465 - 470.

Reina, G., Milella, A., Galati, R., 2017. Terrain assessment for precision agriculture using vehicle dynamic modelling. Biosyst Eng 162, 124 - 139.

Sture, Ø., Øye, E.R., Skavhaug, A., Mathiassen, J.R., 2016. A 3D machine vision system for quality grading of Atlantic salmon. Comput Electron Agr 123, 142 - 148.

Srbinovska, M., Gavrovski, C., Dimcev, V., Krkoleva, A., Borozan, V., 2015. Environmental parameters monitoring in precision agriculture using wireless sensor networks. J Clean Prod 88, 297 - 307.

Su, Q., Kondo, N., Li, M., Sun, H., Al Riza, D.F., 2017. Potato feature prediction based on machine vision and 3D model rebuilding. Comput Electron Agr 137, 41 - 51.

Tang, J., Woods, M., Cossell, S., Liu, S., Whitty, M., 2016. Non-Productive Vine Canopy Estimation through Proximal and Remote Sensing. IFAC-PapersOnLine 49, 398 - 403.

Terribile, F., Bonfante, A., D'Antonio, A., De Mascellis, R., De Michele, C., Langella, G. et al., 2017. A geospatial decision support system for supporting quality viticulture at the landscape scale. Comput Electron Agr 140, 88 - 102.

Weiss, M., Baret, F., 2017. Using 3D Point Clouds Derived from UAV RGB Imagery to Describe Vineyard 3D Macro-Structure. Remote Sens 9, 111.

Zarco-Tejada, P.J., Diaz-Varela, R., Angileri, V., Loudjani, P., 2014. Tree height quantification using very high resolution imagery acquired from an unmanned aerial vehicle (UAV) and automatic 3D photo-reconstruction methods. Eur J Agron 55, 89 - 99.

Zhang, N., Wang, M., Wang, N., 2002. Precision agriculture—a worldwide overview. Comput Electron Agr 36, 113 - 132.